J. Fluid Mech. (2017), *vol.* 811, R2, doi:10.1017/jfm.2016.767

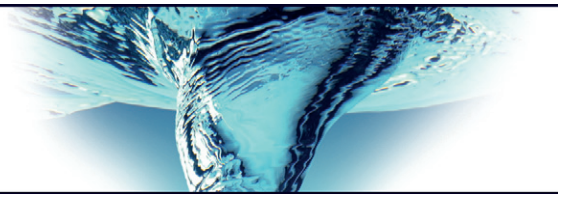

Geometrical shock dynamics for magnetohydrodynamic fast shocks

W. Mostert[1,†], D. I. Pullin[1], R. Samtaney[2] and V. Wheatley[3]

[1]Graduate Aerospace Laboratories, California Institute of Technology, CA 91125, USA

[2]Mechanical Engineering, Physical Science and Engineering Division, King Abdullah University of Science and Technology, Thuwal 23955-6900, Saudi Arabia

[3]School of Mechanical and Mining Engineering, University of Queensland, QLD 4072, Australia

(Received 2 September 2016; revised 25 October 2016; accepted 10 November 2016; first published online 12 December 2016)

We describe a formulation of two-dimensional geometrical shock dynamics (GSD) suitable for ideal magnetohydrodynamic (MHD) fast shocks under magnetic fields of general strength and orientation. The resulting area–Mach-number–shock-angle relation is then incorporated into a numerical method using pseudospectral differentiation. The MHD-GSD model is verified by comparison with results from nonlinear finite-volume solution of the complete ideal MHD equations applied to a shock implosion flow in the presence of an oblique and spatially varying magnetic field ahead of the shock. Results from application of the MHD-GSD equations to the stability of fast MHD shocks in two dimensions are presented. It is shown that the time to formation of triple points for both perturbed MHD and gas-dynamic shocks increases as ϵ^{-1}, where ϵ is a measure of the initial Mach-number perturbation. Symmetry breaking in the MHD case is demonstrated. In cylindrical converging geometry, in the presence of an azimuthal field produced by a line current, the MHD shock behaves in the mean as in Pullin *et al.* (*Phys. Fluids*, vol. 26, 2014, 097103), but suffers a greater relative pressure fluctuation along the shock than the gas-dynamic shock.

Key words: compressible flows, shock waves, MHD and electrohydrodynamics

1. Introduction

Geometrical shock dynamics (GSD) is a semianalytical technique which can be used to approximate the motion of shock waves without the need to calculate a global downstream flow (Chisnell 1957; Whitham 2011). It has proven to be a useful tool to examine shock behaviour in various physical contexts. Geometrical shock dynamics has been used to examine the stability of planar and converging cylindrical gas-dynamic shocks (Whitham 2011), incorporated into various numerical

† Email address for correspondence: wouter.mostert@uqconnect.edu.au

methods (Henshaw, Smyth & Schwendeman 1986; Schwendeman 1993), adapted to problems of shock motion through a stratified flow (Schwendeman 1988), and to certain one-dimensional problems of magnetohydrodynamics (MHD) in the presence of a magnetic field whose angle is fixed perpendicular to the direction of shock motion (Whitham 1957; Pullin *et al.* 2014; Mostert *et al.* 2016).

This last-cited application in the dynamics of MHD shocks is of particular interest since it is known that the Richtmyer–Meshkov instability, a shock-driven interfacial instability (Brouillette 2002) prominent in contexts such as inertial-confinement fusion (Lindl *et al.* 2014), may be suppressed in ideal MHD by the transport of vorticity by MHD waves (Samtaney 2003; Wheatley, Pullin & Samtaney 2005*a*,*b*; Wheatley *et al.* 2014; Mostert *et al.* 2015), or by the Lorentz force (Cao *et al.* 2008), depending on the particular flow configuration.

The purpose of the present work is to develop a shock-dynamics approach for fast-mode MHD shocks in multidimensions under conditions of general non-uniform field strength and orientation ahead of the shock. Section 2 develops the model as follows. In § 2.1, the canonical non-uniform shock-tube problem is formulated for ideal MHD in the general case where the field has components both normal and tangential to the shock, leading to an area–Mach-number–field-angle–distance (A–M–ϕ–x) relation. In § 2.2, this relation is used to construct a GSD method for two-dimensional MHD shock flow, which is developed in § 2.3 into a numerical method following Schwendeman (1993). We verify the model, in § 3, by comparison with results using a full nonlinear finite-volume solver (Samtaney *et al.* 2005) for MHD cylindrically symmetric shock collapse. In § 4, we utilize the GSD-MHD method to investigate the time to formation of shock-shocks (discontinuities in the shock curvature) produced by small Mach-number perturbations on initially planar MHD shocks. A brief theoretical analysis is also discussed. Finally, § 5 applies the MHD-GSD technique to the stability of a converging MHD shock in an azimuthal field produced by a line current.

2. Geometrical shock dynamics for fast MHD shocks

2.1. *One-dimensional multicomponent shock flow*

In the passage of a gas-dynamic shock moving along a tube of non-uniform area, the shock Mach number M and the varying tube area A may be related approximately by Whitham's characteristic rule of shock dynamics (Whitham 2011). Here, the characteristic equation for the fluid Euler equations is first written for the C^+ or C^- characteristic as a function of the tube area A, assuming quasi-one-dimensional flow, and, second, the flow quantities appearing in this equation are interpreted as postshock conditions given by the Rankine–Hugoniot jump conditions as a function of the upstream flow state. This leads to an A–M relation. Although Whitham applies his initial derivation to a physical shock tube, in the later generalization to two or higher dimensions, the tube walls are interpreted approximately as rays normal to the shock. Presently we follow this interpretation, which is discussed further subsequently.

In ideal MHD in the presence of a magnetic field oblique to the shock, the jump conditions lead to discontinuous changes in components of physical variables tangential to the shock. In order to admit both normal and tangential magnetic-field components, and hence tangential velocities downstream of the shock, we consider a one-dimensional multicomponent (1D-MC) formulation. Specifically, for a quasi-one-dimensional flow with shock-normal coordinate x, we allow non-zero velocity and magnetic-field components in the orthogonal direction y (along the shock surface,

perpendicular to the shock normal), but require that these be functions only of x. The presence of a tangential velocity jump across the shock, which is not present in ordinary gas dynamics, means that downstream of the shock, particle paths and shock-normal rays separate. We refer to this as downstream path–ray divergence. This may perhaps be interpreted as shock movement in a tube with porous walls. Noting that shock dynamics does not represent the flow downstream of the shock, downstream path–ray divergence would appear to be unimportant, and, for this reason, we prefer the strict ray-tube interpretation. This is revisited in § 3. The 1D-MC MHD equations are then

$$\frac{\partial \boldsymbol{v}}{\partial t} + \boldsymbol{A}\frac{\partial \boldsymbol{v}}{\partial x} + \frac{A'(x)}{A(x)}\boldsymbol{s} = 0, \tag{2.1}$$

where $\boldsymbol{v} = \{\rho, u, v, p, B_x, B_y\}^{\mathrm{T}}$ is the primitive vector, with ρ the density, u, v the velocities normal and tangential to the shock, B_x, B_y the field components normal and tangential to the shock and p the pressure; $\boldsymbol{s}$ is the vector of source terms,

$$\boldsymbol{s} = \left\{ \rho u, \frac{B_y^2 - \rho v^2}{\rho}, \frac{\rho u v - B_x B_y}{\rho}, \rho a^2 u, 0, 0 \right\}^{\mathrm{T}}, \tag{2.2}$$

where a is the thermodynamic sound speed. The coefficient matrix $\boldsymbol{A}$ is

$$\boldsymbol{A} = \begin{pmatrix} u & \rho & 0 & 0 & 0 & 0 \\ 0 & u & 0 & 1/\rho & 0 & B_y/\rho \\ 0 & 0 & u & 0 & 0 & -B_x/\rho \\ 0 & p\gamma & 0 & u & 0 & 0 \\ 0 & 0 & 0 & 0 & 0 & 0 \\ 0 & B_y & -B_x & 0 & -v & u \end{pmatrix}, \tag{2.3}$$

and, for the C^+ eigenvalue $u + c_f$ of $\boldsymbol{A}$, the associated left eigenvector is

$$\boldsymbol{e}_L = \left\{ 0, \frac{\rho c_f^2 - B_x^2}{c_f}, -\frac{B_x B_y}{c_f}, \left(1 - \frac{B_x^2}{\rho c_f^2}\right), -\frac{v B_y}{u + c_f}, B_y \right\}^{\mathrm{T}}, \tag{2.4}$$

leading to the equation on the C^+ characteristic,

$$\boldsymbol{e}_L \cdot \left(\frac{\mathrm{d}\boldsymbol{v}}{\mathrm{d}x} + \frac{1}{u + c_f}\frac{1}{A}\frac{\mathrm{d}A}{\mathrm{d}x}\boldsymbol{s} \right) = 0, \quad c_f^2 = \frac{1}{2\rho}\left(\gamma p + B^2 + \sqrt{(\gamma p + B^2)^2 - 4\gamma p B_x^2} \right), \tag{2.5a,b}$$

where $B^2 = B_x^2 + B_y^2$. All quantities have been non-dimensionalized according to Goedbloed, Keppens & Poedts (2010). Generally, the jump conditions given by Wheatley *et al.* (2005*a*) may be written as $q = q(M, x, \phi; \gamma)$, where ϕ is the local orientation of the field to the shock normal and γ is the thermodynamic specific heat ratio. Use of the chain rule for x-derivatives of (2.5) applied to the shock jump conditions leads to a differential form of the A–M–ϕ–x relation,

$$\frac{\mathrm{d}}{\mathrm{d}x} = \frac{\partial}{\partial x} + \frac{\partial}{\partial M}\frac{\mathrm{d}M}{\mathrm{d}x} + \frac{\partial}{\partial \phi}\frac{\mathrm{d}\phi}{\mathrm{d}x}, \tag{2.6}$$

$$\frac{\mathrm{d}M}{\mathrm{d}x} = -\frac{\boldsymbol{e}_L \cdot \left(\dfrac{\partial \boldsymbol{v}}{\partial \phi}\dfrac{\mathrm{d}\phi}{\mathrm{d}x} + \dfrac{\partial \boldsymbol{v}}{\partial x} + \dfrac{1}{A}\dfrac{\mathrm{d}A}{\mathrm{d}x}\dfrac{1}{u + c_f}\boldsymbol{s} \right)}{\boldsymbol{e}_L \cdot \dfrac{\partial \boldsymbol{v}}{\partial M}}. \tag{2.7}$$

For a shock-tube problem with known $A(x)$, field strength and orientation, (2.7) may be solved analytically or numerically. Presently, due to complexity, we use the latter. In (2.7), M may be either gas-dynamic or magnetosonic. For numerical convenience and compatibility with the jump conditions of Wheatley *et al.* (2005*a*), we interpret it explicitly as the gas-dynamic Mach number. The relation (2.7) is used to close the equations of §§ 2.2 and 2.3 below.

2.2. *Equations of two-dimensional GSD*

The equations of GSD are (Whitham 2011)

$$\boldsymbol{\nabla}\cdot((M/A)\boldsymbol{\nabla}\alpha)=0, \quad M=1/|\boldsymbol{\nabla}\alpha|, \quad A=f(M,\phi,x), \tag{2.8a–c}$$

where (2.8*c*) has been interpreted in terms of the MHD formulation above, and is presently computed numerically (γ-dependence suppressed for convenience). Here, α is a shock-normal coordinate that is time-like, given by $\alpha(\boldsymbol{x}) = a_0 t$. With this definition, curves of constant α are instantaneous shock surfaces (Whitham 2011), characterized by the gas-dynamic Mach number M. Equation (2.8) describes a second-order system of hyperbolic partial differential equations, which describe wave motion along the shock surface. In this way, disturbances can propagate along and steepen into 'shock-shocks' (Whitham 2011) on the shock surface, which correspond physically to the formation of triple points.

2.3. *Numerical method*

We adapt the method of Schwendeman (1993) in two dimensions, which we briefly present. We introduce an orthogonal curvilinear coordinate system (ξ, η) with scale factors (σ, τ) so that (2.8*a*) becomes

$$\frac{\partial}{\partial\xi}(FU)+\frac{\partial}{\partial\eta}(GV)=0, \tag{2.9}$$

with

$$U=\frac{1}{\sigma}\frac{\partial\alpha}{\partial\xi}, \quad V=\frac{1}{\tau}\frac{\partial\alpha}{\partial\eta}, \quad F=\tau\frac{M}{A}, \quad G=\sigma\frac{M}{A}, \tag{2.10a–d}$$

along with (2.8*b*) and (2.8*c*),

$$M=(U^2+V^2)^{-1/2}, \quad A=f(M,\phi,x). \tag{2.11a,b}$$

We discretize on the domain $\xi > 0$, $0 < \eta < 1$ and apply upwind differencing in ξ and pseudospectral differentiation in η, assuming the primary motion of the shock to be in ξ. The equations (2.9) are advanced in ξ, solving implicitly for α with a Crank–Nicolson method.

We evaluate $A(M, \phi, x)$, closing (2.9), by advancing the form of the ordinary differential equation (ODE) (2.7) adapted for this problem as

$$\boldsymbol{e}_L\cdot\left[\frac{\partial\boldsymbol{v}}{\partial x}\,\mathrm{d}x+\frac{\partial\boldsymbol{v}}{\partial\phi}\,\mathrm{d}\phi+\frac{\partial\boldsymbol{v}}{\partial M}\mathrm{d}M+\frac{1}{u+c_f}\boldsymbol{s}\frac{\mathrm{d}A}{A}\right]=0 \tag{2.12}$$

with an ODE solver, where $\mathrm{d}x = M\mathrm{d}\alpha$ and $\partial\boldsymbol{v}/\partial x = M\boldsymbol{\nabla}\boldsymbol{v}\cdot(\boldsymbol{\nabla}\alpha)$. The present pseudospectral technique in η uses periodic boundaries with an exponential filter applied during the differentiation steps. This filter decreases the error associated with the Gibbs phenomenon when shock-shocks form (Don 1994) and with pseudospectral aliasing (Hou & Li 2007).

3. Comparison of MHD-GSD with full ideal MHD

We test the model with a nonlinear second-order finite-volume solver for the full ideal MHD equations (CMHD) (Samtaney *et al.* 2005). The test case is cylindrical shock collapse in the presence of a spiral magnetic field defined by

$$\boldsymbol{B}(r) = \frac{1}{\sqrt{b^2+1}}\left(\frac{b}{r}\hat{\boldsymbol{e}}_r + \frac{1}{r}\hat{\boldsymbol{e}}_\theta\right), \tag{3.1}$$

where b is a real positive parameter. This spiral magnetic field is solenoidal on $r > 0$. For appropriate choices of b, it allows an oblique orientation of the field to the collapsing shock normal. Behind the shock, particle paths are not radial and do not coincide with rays normal to the shock surface. This then tests the effect of downstream path–ray divergence on the present formulation of MHD-GSD.

The initial conditions for the cylindrical shock are an initial radius of $r_0 = 100$ at an initial preshock magnetosonic Mach number of $M_{f0} = 2$, and we consider values of $b = 0.1, 1.0, 3.0, 10.0$. For the numerical method used in the GSD code, the scale factors are $\sigma = r_0 e^{-\xi}$, $\tau = 2\pi r_0 e^{-\xi}$.

The key variables for comparison are the M_f, postshock variables p, tangential magnetic field B_θ, and tangential velocity u_θ, the latter two of which sufficiently account for the oblique postshock particle paths. The comparison is shown in figure 1. The largest discrepancy is observed in postshock pressure $p(r)$ of 9 % in the peak value. This difference between shock dynamics and the full nonlinear equations is consistent with that seen in previous studies such as Pullin *et al.* (2014), suggesting that the introduction of the oblique field into MHD shock dynamics has not significantly affected the effectiveness of the approximation. Presently, the presence of downstream path–ray divergence does not appear to compromise the performance of MHD-GSD, suggesting that this is not an important feature of the general GSD framework.

4. Stability of plane fast MHD shocks

Consider a simple problem of planar shock propagation in an infinitely wide channel. Planar gas-dynamic shocks are known to be stable in the sense that small initial perturbations decay to zero amplitude over large time (Whitham 2011). The stability of planar MHD shocks is less well studied, but see Trakhinin (2003). Whitham (2011) argues briefly that an initially smooth disturbance on a planar gas-dynamic shock will undergo wave steepening so that discontinuities on the shock surface, or shock-shocks, form following an initial disturbance.

We consider initially planar shocks with sinusoidal perturbation in Mach number $M_0 = M_r[1 + \epsilon \sin(2\pi y/\lambda)]$, where y is the dimension along the initial planar shock, and $M_r = 1.8$, $\lambda = 1$, $\epsilon = 0.06$ in this case. Here, ϵ is chosen to expose a sizeable perturbation whose motion on the shock may be discerned easily. Figure 2(*a*) shows the resulting flow pattern for gas-dynamic shocks. The shock travels from left to right and is shown with thick vertical lines, with perturbations on the shock surface exaggerated fivefold. Local M, whose contours can be considered to be characteristics of the disturbance motion along the shock, is shown by shaded colour. Shock-shocks first occur where a kink, or point of infinite curvature, appears on the shock profile, accompanied by the appearance of a discontinuity in M. The onset of shock-shocks can be seen by M contour-gradient steepening followed by the diamond-like formations signalling M discontinuities. These diamonds appear

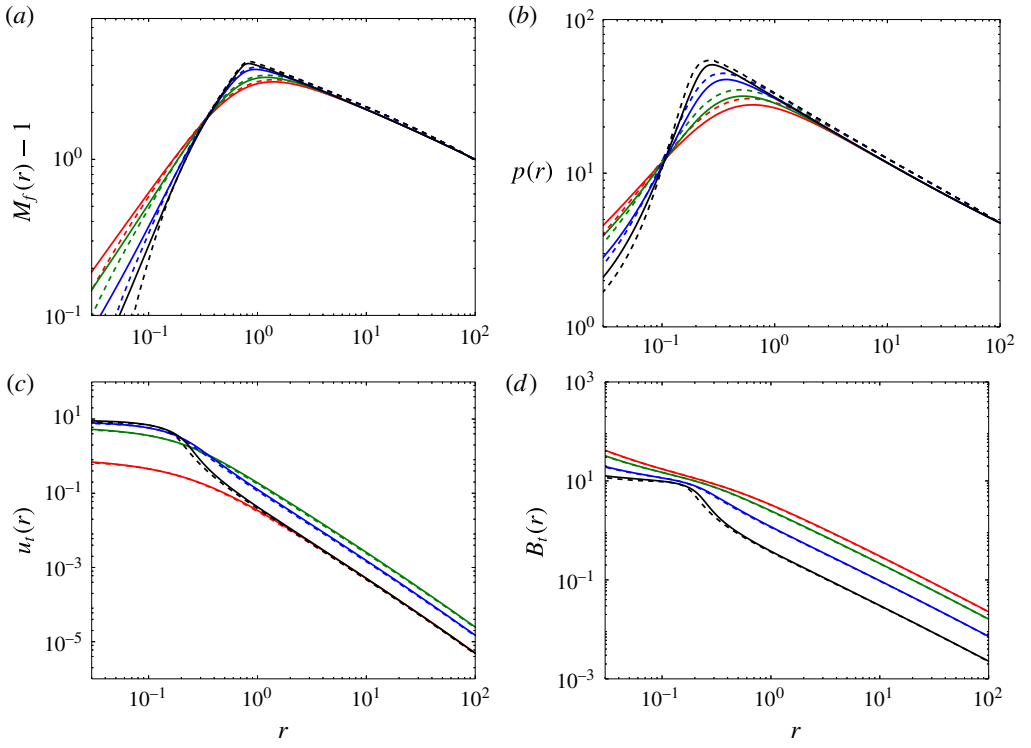

FIGURE 1. Comparison between MHD-GSD and CMHD of fast magnetosonic Mach number and three key postshock variables for cylindrical shock collapse in a spiral magnetic field: —, MHD-GSD; - -, CMHD. The CMHD results run with 8000 cells in r, the GSD results at $\Delta\xi = 1 \times 10^{-3}$. On the far left of each panel (a), (b), (d), from top to bottom, $b = 0.1, 1.0, 3.0, 10.0$; (c), from bottom to top, $b = 0.1, 1.0, 3.0, 10.0$.

symmetric around their major axes, since disturbances travelling up and down the shock surface have the same strengths and speeds.

Figure 2(b), however, shows an equivalent MHD shock for upstream $|B| = 1.55, \phi = 0.199$ radians, perturbed with the same variation in M_0. The general pattern is similar to the gas-dynamic case but there is a clear directional preference in the developed flow. This symmetry-breaking effect is an interesting feature of MHD shocks in oblique magnetic fields, and is caused by the generation of a non-zero downstream tangential velocity that intensifies with increasing magnetic-field strength and decreasing orientation. Indeed, the conditions for figure 2(b) are chosen to make this effect particularly noticeable.

We now seek to quantify the time $t_B(\epsilon)$ to first shock-shock formation. A sequence of GSD calculations was performed for both gas-dynamic and MHD shocks over a range of ϵ. Shock-shocks are detected as discontinuities in M by an edge-detection algorithm (Gelb & Tadmor 2000, 2006) with a minmod limiter giving a switch between an exponential concentration factor kernel (high order) away from shock-shocks and a first-order polynomial kernel close to shock-shocks, limiting spurious oscillations in the detector. A nonlinear enhancement technique was used to remove small jumps on the grid scale in the discretized solution while allowing $O(M_r\epsilon)$ jumps, which correspond to shock-shocks, using a tuning parameter

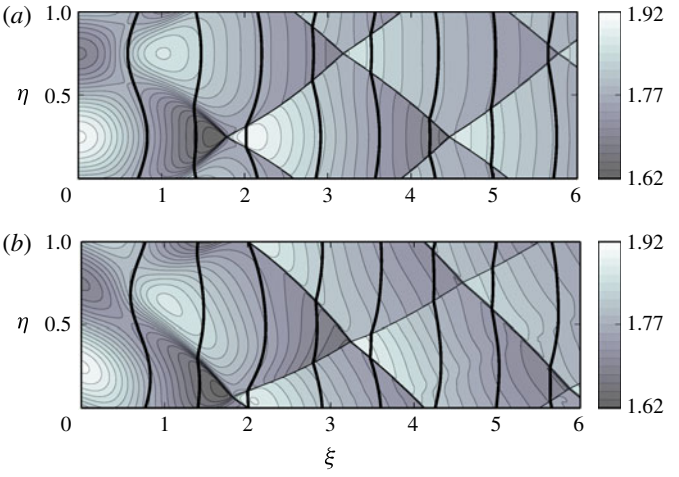

FIGURE 2. Contours showing successive shock position, moving left to right. Shock position is given by thick vertical lines with perturbation amplitude exaggerated fivefold and local M by faint contours and colour. The colour at a given location shows the shock M when it passed through that location. (*a*) Gas-dynamic shock; (*b*) MHD shock, $|B|_0 = 1.55$, $\phi_0 = 0.199$. Shocks are initially flat, but perturbed sinusoidally in M with $\epsilon = 0.06$, $M_r = 1.8$.

chosen to reflect the expected minimum magnitude of the shock-shock when it forms. The time t_B is when the edge detector first gives a non-zero result, and is largely insensitive to plausible choices of the tuning parameter. Parameters used for the nonlinear enhancement technique give resolution-converged results with $<1\,\%$ discrepancy between resolutions of $N_\eta = 2048$ and 4096.

We use uniform upstream magnetic fields of strength $B_0 = 0.5$, 1, 1.5 and initial upstream orientation $\phi = \pi/4$, $\pi/2$, along with a gas-dynamic case. Values of $\epsilon = 4 \times 10^{-3}$, 6×10^{-3}, 8×10^{-3}, 1×10^{-2}, 2×10^{-2}, 4×10^{-2}, 8×10^{-2} are considered with $M_r = 1.8$. The scale factors in the numerical method are $\sigma = \tau = 1$, and the numerical resolution $\Delta\xi$, $\Delta\eta$ for these problems is $\epsilon/20$, $\lambda/2048$. Figure 3 shows variation of t_B over the ϵ considered. A power law ϵ^{-m} with exponent close to $m = -1$ is observed across all cases, independent of field strength or orientation. This result can be understood by developing analysis alluded to in passing by Whitham (2011). The characteristic form of the shock-dynamic equations (2.8) may be written in coordinates (α, β) normal and tangential to the shock as

$$\left(\frac{\partial R}{\partial \alpha} \pm c(M)\frac{\partial R}{\partial \beta}\right) = 0, \quad R = \left(\theta \pm \int \frac{\mathrm{d}M}{Ac}\right), \quad c(M) = \sqrt{\frac{-M}{A(M)A'(M)}}, \quad (4.1a\text{–}c)$$

where R is a Riemann invariant and θ describes the angle of the local shock normal to some reference axis (for example x). Here and subsequently, primes indicate differentiation. In (4.1), the ϕ, x dependence in $A(M, \phi, x)$ has been suppressed for clarity.

In gas dynamics, M, c have smooth representations $M(R), c(R)$. We assume that this holds for MHD with $M_f > 1$. Now, considering only one family of characteristics and ignoring wave interactions, a nonlinear wave equation can be obtained with wavespeed

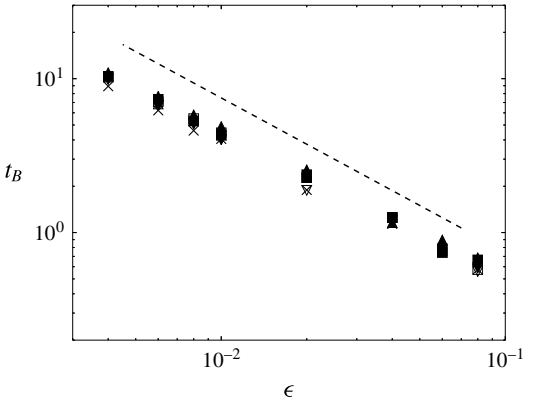

FIGURE 3. Shock-shock formation times t_B over initial Mach-number relative disturbance amplitude ϵ: $\times$, gas-dynamic shock; $\blacktriangledown$, $\blacksquare$, $\blacktriangle$, upstream $|B| = 0.5, 1.0, 1.5$; filled, unfilled, upstream field orientation $\phi = \pi/2, \pi/4$; $--$, power law, $t_B \sim \epsilon^{-1}$ expected from the theoretical analysis.

$c(R)$,

$$\frac{\partial R}{\partial \alpha} + c(R)\frac{\partial R}{\partial \beta} = 0, \quad \frac{\partial R}{\partial \alpha} + \frac{\partial (Q(R))}{\partial \beta} = 0, \tag{4.2a,b}$$

where (4.2*b*) is a conservation form with $Q'(R) = c(R)$. Now, for an initial condition $R(\beta_0)$ at $\alpha = 0$, (4.2) has a continuous solution

$$R = R(\beta_0) \text{ or } c = c(R(\beta_0)) \quad \text{on } \beta = \beta_0 + c(R(\beta_0))\alpha, \tag{4.3}$$

and at discontinuities (shock-shocks) with speed S the conservation law requires

$$S = \frac{Q(R_2) - Q(R_1)}{R_2 - R_1} = \frac{1}{2}(c(R_1) + c(R_2)), \tag{4.4}$$

where subscripts 1, 2 indicate upstream and downstream states respectively and the right-hand side of (4.4) follows from linearizing $c(R)$, allowing quadratic $Q(R)$. The solution can thus be written entirely in terms of c, which in this form is also a weak solution to the inviscid Burgers equation (and conservation form), simplifying the problem further,

$$\frac{\partial c}{\partial \alpha} + c(\beta)\frac{\partial c}{\partial \beta} = 0, \quad \frac{\partial c}{\partial \alpha} + \frac{\partial}{\partial \beta}\left(\frac{1}{2}c^2\right) = 0. \tag{4.5a,b}$$

The first value α_B at which shock-shocks form can be calculated as a function of the initial distribution $c(\beta_0)$ as (Whitham 2011) $\alpha_B = 1/|c'(\beta_0)|$, corresponding, by definition of α, to a shock-shock formation time $t_B = (a_0|c'(\beta_0)|)^{-1}$.

For an initially sinusoidal, or indeed any continuous periodic distribution of c on the shock with amplitude proportional to ϵ, this implies $t_B \sim 1/\epsilon$ to leading order, in agreement with the numerical GSD results. This indicates that t_B depends only upon the initial distribution in c and is independent of the A–M relation and therefore of whether the shock is of gas-dynamic or MHD type. Higher-order effects would include the influence of the other characteristic family corresponding to the minus sign in (4.1), which has been ignored here.

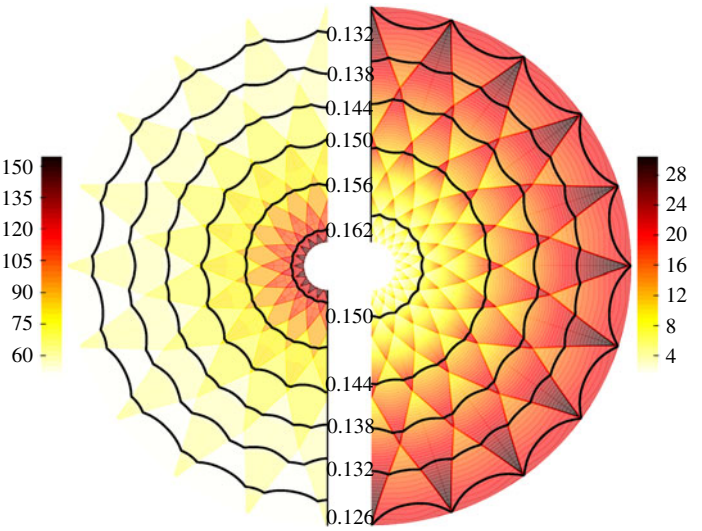

FIGURE 4. Contour maps for cylindrical converging gas-dynamic (left) and MHD (right) shocks. The azimuthal extent of the simulation domain is one wavelength. The inner and outer radii are $r_{in} = 0.027$, $r_{out} = 0.3$. Black contours show successive shock positions, with labels on the top (bottom) half corresponding to gas-dynamic (MHD) shock positions $\alpha \propto t$. Shock perturbation amplitudes are exaggerated fourfold. The colour maps indicate local postshock pressure (note the different colour scales). The colour at a given location shows the pressure downstream of the shock as it passes that location. While both shocks exhibit the same polygonal instability, the MHD shock sees a progressive decrease in postshock pressure, in direct contrast to the gas-dynamic shock, and accelerates at a greater rate.

5. Stability of converging cylindrical fast MHD shocks

We now consider stability of cylindrical converging MHD shocks. The azimuthal field is given by (3.1) with $b = 0$ and the shock is initialized as in § 4 with $M_r = 5.0$, $\epsilon = 0.06$. Scale factors are set as in § 3. The simulation is run on one wavelength, $\lambda = 2\pi/k$, with wavenumber $k = 20$ and initial radius $r_0 = 1$. These conditions are chosen to promote short time to shock-shock formation. The resolution is $N_\eta = 1024$, $\Delta\xi = 0.003$ (recall that ξ, η are curvilinear coordinates). Figure 4 shows the gas-dynamic (left) and MHD (right) shock convergence between the inner and outer radii $r_{in} = 0.027$, $r_{out} = 0.3$ and extended periodically to 10 wavelengths around a half-circle. The colour shows the local postshock pressure and the black line values show α, which is proportional to t, for the shock position contours.

The MHD shock accelerates faster than the gas-dynamic shock. Indeed, figure 5 shows that the gas-dynamic Mach number averaged along the shock approaches an $\bar{R}^{-1}$ asymptote in the MHD case, where $\bar{R}$ is the mean shock radius, compared with $\bar{R}^{-1/n}$ for the gas-dynamic shock, with $n = 1 + 2/\gamma + (2\gamma/(\gamma - 1))^{1/2}$ and $1/n = 0.225425$ for $\gamma = 5/3$ (Whitham 2011). Moreover, unlike the gas-dynamic shock, where the postshock pressure p becomes singular as $\bar{R} \to 0$, the converging MHD shock sees $p \sim 1 + A\bar{R} \ldots$, $\bar{R} \to 0$, where A is a positive constant, as in the unperturbed result (Pullin *et al.* 2014). Figure 6(*a*) shows that both shocks have similar profiles in $\Delta R/\bar{R}$, where $\Delta R = R_{max} - R_{min}$ is the peak-to-trough variation of shock radius R along its surface, exhibiting the weak instability noted by Schwendeman (1993) and others.

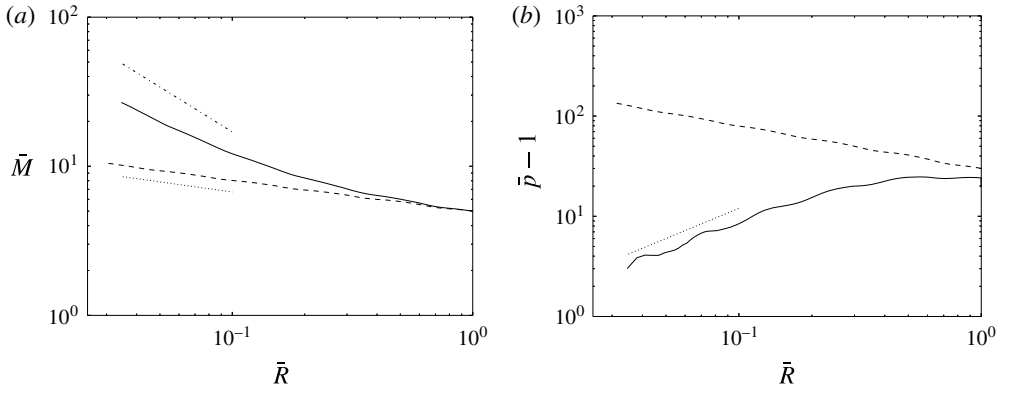

FIGURE 5. Variation of mean Mach number, pressure over radius: (*a*) —, $\bar{M}$ for MHD shocks; – –, $\bar{M}$ for gas-dynamic shocks; · · · , $M \sim \bar{R}^{-1/n}$, gas-dynamic asymptote; –·–·, $M \sim \bar{R}^{-1}$, MHD asymptote; (*b*) —, $\bar{p}-1$ for MHD shocks; – –, $\bar{p}-1$ for gas-dynamic shocks; · · · , $\bar{p}-1 \sim \bar{R}$, MHD asymptote.

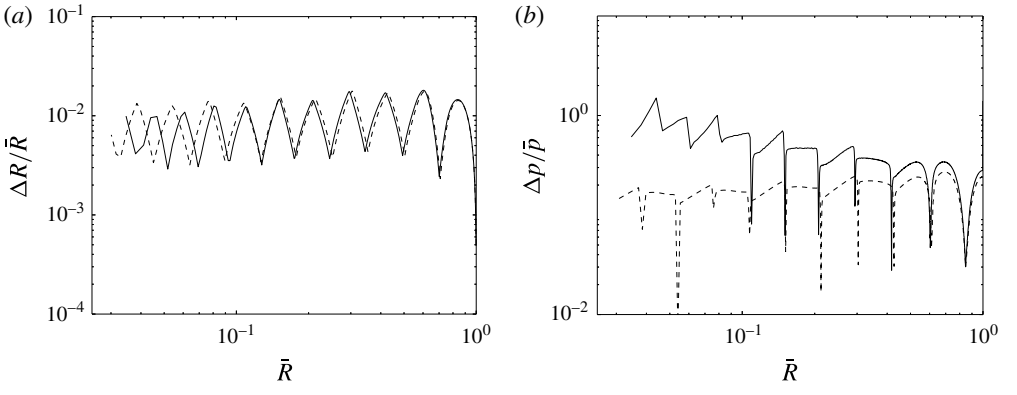

FIGURE 6. Graphs of shock variation in geometry, $\Delta R/\bar{R}$ (*a*) and postshock pressure $\Delta p/\bar{p}$ (*b*), on the shock as it converges: —, MHD shock; – –, gas-dynamic shock. Here, ΔR is the total variation of shock radius along its surface and $\bar{R}$ is its mean radius; $\Delta p/\bar{p}$ is defined similarly.

Figure 6(*b*) shows that the MHD shock instability differs from the gas-dynamic shock in the variation of postshock pressure, $\Delta p/\bar{p}$, defined similarly, which grows with decreasing $\bar{R}$ in the MHD case while remaining sensibly constant for the gas-dynamic shock. In addition to the weakening of the shock on collapse in the mean, the MHD shock then also shows a greater relative pressure fluctuation in comparison to the gas-dynamic case. We remark that the hodograph transformation of Whitham (2011) admits analysis of the perturbed shock collapse for the gas-dynamic case but is not simply extensible to the present MHD case.

6. Concluding remarks

A formulation of GSD has been developed for fast shocks in ideal MHD and implemented numerically using a pseudospectral method. Application to a cylindrically

symmetric converging MHD shock in the presence of a non-uniform upstream field at an oblique angle gives satisfactory comparison with results from numerical solutions of the full MHD equations. A novel application to the nonlinear stability of planar fast MHD shocks indicates a time to shock-shock formation inversely proportional to the initial Mach-number perturbation amplitude, in agreement with a simple model based on the Burgers equation. A further comparison between converging MHD and gas-dynamic shocks exposes a notable difference in the postshock pressure variation along the shock, showing a greater growth in pressure fluctuation for the MHD case over the gas-dynamic convergence. The present MHD-GSD approach is expected to be useful in studies of general MHD shock behaviour.

Acknowledgements

This research was supported by the KAUST Office of Sponsored Research under award URF/1/2162-01. V.W. holds an Australian Research Council Discovery Early Career Researcher Award (project number DE120102942).

References

BROUILLETTE, M. 2002 The Richtmyer–Meshkov instability. *Annu. Rev. Fluid Mech.* **34** (1), 445–468.

CAO, J., WU, Z., REN, H. & LI, D. 2008 Effects of shear flow and transverse magnetic field on Richtmyer–Meshkov instability. *Phys. Plasmas* **15**, 042102.

CHISNELL, R. F. 1957 The motion of a shock wave in a channel, with applications to cylindrical and spherical shock waves. *J. Fluid Mech.* **2**, 286–298.

DON, W. S. 1994 Numerical study of pseudospectral method in shock wave applications. *J. Comput. Phys.* **110**, 103–111.

GELB, A. & TADMOR, E. 2000 Detection of edges in spectral data II: nonlinear enhancement. *SIAM J. Numer. Anal.* **38** (4), 1389–1408.

GELB, A. & TADMOR, E. 2006 Adaptive edge detectors for piecewise smooth data based on the minmod limiter. *J. Sci. Comput.* **28** (2/3), 279–306.

GOEDBLOED, J. P., KEPPENS, R. & POEDTS, S. 2010 *Advanced Magnetohydrodynamics*. Cambridge University Press.

HENSHAW, W. D., SMYTH, N. F. & SCHWENDEMAN, D. W. 1986 Numerical shock propagation using geometrical shock dynamics. *J. Fluid Mech.* **171**, 519–545.

HOU, T. Y. & LI, R. 2007 Computing nearly singular solutions using pseudo-spectral methods. *J. Comput. Phys.* **226**, 379–397.

LINDL, J., LANDEN, O., EDWARDS, J., MOSES, E. & TEAM, NIC 2014 Review of the National Ignition Campaign 2009–2012. *Phys. Plasmas* **21**, 020501.

MOSTERT, W., PULLIN, D. I., SAMTANEY, R. & WHEATLEY, V. 2016 Converging cylindrical magnetohydrodynamic shock collapse onto a power-law-varying line current. *J. Fluid Mech.* **793**, 414–443.

MOSTERT, W., WHEATLEY, V., SAMTANEY, R. & PULLIN, D. I. 2015 Effects of magnetic fields on magnetohydrodynamic cylindrical and spherical Richtmyer–Meshkov instability. *Phys. Fluids* **27**, 104102.

PULLIN, D. I., MOSTERT, W., WHEATLEY, V. & SAMTANEY, R. 2014 Converging cylindrical shocks in ideal magnetohydrodynamics. *Phys. Fluids* **26**, 097103.

SAMTANEY, R. 2003 Suppression of the Richtmyer–Meshkov instability in the presence of a magnetic field. *Phys. Fluids* **15** (8), L53–L56.

SAMTANEY, R., COLELLA, P., LIGOCKI, T. J., MARTIN, D. F. & JARDIN, S. C. 2005 An adaptive mesh semi-implicit conservative unsplit method for resistive MHD. *J. Phys.: Conf. Ser.* **16** (1), 40–48.

SCHWENDEMAN, D. 1988 Numerical shock propagation in non-uniform media. *J. Fluid Mech.* **188**, 383–410.

SCHWENDEMAN, D. W. 1993 A new numerical method for shock wave propagation based on geometrical shock dynamics. *Proc. R. Soc. Lond.* A **441** (1912), 331–341.

TRAKHININ, Y. 2003 A complete 2D stability analysis of fast MHD shocks in an ideal gas. *Commun. Math. Phys.* **236**, 65–92.

WHEATLEY, V., PULLIN, D. I. & SAMTANEY, R. 2005*a* Regular shock refraction at an oblique planar density interface in magnetohydrodynamics. *J. Fluid Mech.* **522**, 179–214.

WHEATLEY, V., PULLIN, D. I. & SAMTANEY, R. 2005*b* Stability of an impulsively accelerated density interface in magnetohydrodynamics. *Phys. Rev. Lett.* **95**, 125002.

WHEATLEY, V., SAMTANEY, R., PULLIN, D. I. & GEHRE, R. M. 2014 The transverse field Richtmyer–Meshkov instability in magnetohydrodynamics. *Phys. Fluids* **26**, 016102.

WHITHAM, G. B. 1957 A new approach to problems of shock dynamics. Part I. Two-dimensional problems. *J. Fluid Mech.* **2**, 145–171.

WHITHAM, G. B. 2011 *Linear and Nonlinear Waves*. Wiley.